

RESEARCH ARTICLE | JANUARY 09 2026

AO-HEOM: A computational platform for non-Markovian quantum dissipative dynamics in atomic orbital spaces

Special Collection: [Computational Spectroscopy](#)

Yankai Zhang ; Yoshitaka Tanimura  



J. Chem. Phys. 164, 022501 (2026)

<https://doi.org/10.1063/5.0312209>



Articles You May Be Interested In

Hierarchical equations of motion for multiple baths (HEOM-MB) and their application to Carnot cycle

J. Chem. Phys. (October 2024)

Thermodynamic quantum Fokker–Planck equations and their application to thermostatic Stirling engine

J. Chem. Phys. (September 2024)

mqsqd: A matrix product state based Python package to simulate closed and open system quantum dynamics

J. Chem. Phys. (September 2024)



The Journal of Chemical Physics

Special Topics Open for Submissions

[Learn More](#)

AO-HEOM: A computational platform for non-Markovian quantum dissipative dynamics in atomic orbital spaces

Cite as: J. Chem. Phys. **164**, 022501 (2026); doi: [10.1063/5.0312209](https://doi.org/10.1063/5.0312209)

Submitted: 14 November 2025 • Accepted: 22 December 2025 •

Published Online: 9 January 2026



View Online



Export Citation



CrossMark

Yankai Zhang  and Yoshitaka Tanimura ^{a)} 

AFFILIATIONS

Department of Chemistry, Graduate School of Science, Kyoto University, Kyoto 606-8502, Japan

Note: This paper is part of the Special Topic on Computational Spectroscopy.

^{a)} Author to whom correspondence should be addressed: tanimura.yoshitaka.5w@kyoto-u.jp

ABSTRACT

Building upon our previous implementation for the hydrogen atom [Y. Zhang and Y. Tanimura, J. Chem. Phys. **163**, 184108 (2025)], we have developed source code for atomic orbital–hierarchical equations of motion (AO-HEOM), a quantum mechanical framework based on HEOM formulated within an AO basis. This method enables numerically “exact” simulations of atomic systems coupled to three independent thermal baths, under both isotropic and anisotropic conditions, while preserving rotational symmetry. AO-HEOM rigorously accounts for system–bath entanglement, which is critical for describing the quantum nature of environmental interactions. Incorporating spatial bath degrees of freedom significantly increases the computational cost in the HEOM formalism because of the proliferation of electronic states at high temperatures and the inclusion of Matsubara frequency terms at low temperatures. To address this challenge, we developed a graphics processing unit-accelerated implementation. As a demonstration, we computed the emission spectra of He I and He II atoms. The source code is broadly applicable to atomic systems and enables detailed analysis of electronic transitions in thermal environments.

Published under an exclusive license by AIP Publishing. <https://doi.org/10.1063/5.0312209>

I. INTRODUCTION

Open quantum dynamics theory, originating from Bloch’s foundational work,¹ has evolved through the study of simple systems such as spins,² two-level atoms,^{3,4} and Brownian oscillators.^{5,6}

Advances in experimental techniques, such as single-atom spectroscopy,^{7–9} single-molecule spectroscopy,¹⁰ and ultrafast nonlinear spectroscopy,¹¹ have made simulation techniques for quantum phenomena in complex systems, including nanodevices and photosynthetic systems, increasingly important. The key to treating such systems lies in the quantum coherence (entanglement) between the system of interest and its thermal bath (“bath entanglement”).^{12,13} For instance, even in simple spin-boson and Brownian models, the Markovian assumption, factorization approximation, and rotating wave approximation fail to hold when quantum thermal effects are properly accounted for,^{2,14} particularly because of the inclusion of bath entanglement.^{15,16}

In response to these limitations, several theoretical frameworks have been developed to rigorously and quantitatively

incorporate the influence of the thermal environment. Notably, the hierarchical equations of motion (HEOM)^{17–21} and the quasi-adiabatic path-integral (QUAPI) approach^{22–24} are nonperturbative and non-Markovian methods that have proven particularly effective.

Although computationally expensive, these methodologies have been established and applied to experimentally relevant complex systems characterized by multiple energy levels and multiple thermal baths, such as excitonic²⁵ and electron-conducting systems²⁶ modeled by multiple two-level subsystems, single molecular junctions,^{27–29} and nonadiabatic transition systems involving multidimensional and multilevel potential energy surfaces.³⁰ Current trends are focused on developing computational methods to apply established models to more complex systems and to simulate them.^{31–46}

Although the systems studied have evolved in complexity and nuance, the representation of heat baths has seen little conceptual advancement since the pioneering framework introduced by Bloch. They continue to be idealized as spatially featureless reservoirs, defined only by temperature and a spectral distribution function

(SDF) that encapsulates noise correlation and system–bath coupling strength. This abstraction becomes particularly restrictive in contexts in which the spatial symmetry of the system plays a decisive role in its dynamics.

For instance, while the relaxation dynamics of a classical rigid-body rotor can be described by coupling its rotational degrees of freedom to a harmonic bath, applying the same scheme to a quantum rotor fails to yield discrete rotational levels because the symmetry of the total system is not preserved.^{47,48} Specifically, if the bath does not share the symmetry of the rotor, the entanglement between the system and bath is disrupted as the rotor evolves.

To preserve bath entanglement under rotational transformations, both the system and bath Hamiltonians must possess rotational symmetry. We have thus introduced a framework that embeds bath effects directly into a system of interest via the rotationally invariant system–bath (RISB) model.⁴⁹ This approach, implemented within the HEOM formalism, enables the study of quantum rigid-rotor dynamics in both two-dimensional (2D) and three-dimensional (3D) settings,^{50,51} as well as charge transport in Aharonov–Bohm ring systems.^{52,53} These investigations have primarily focused on motion within spatially constrained geometries.

More recently, we extended this approach to a spherically symmetric atomic system, treating an electron confined by a Coulomb potential as a more fundamental case.⁵⁴ The results revealed phenomena beyond the reach of conventional models based on energy eigenstates and standard thermal baths. In particular, electronic transitions involving higher angular momentum states underwent enhanced thermal relaxation, thereby suppressing Paschen and Brackett transitions, whereas Lyman and Balmer transitions remained discernible in the absorption spectrum.⁵⁴

This paper presents the source code for atomic orbital–hierarchical equations of motion (AO-HEOM), a quantum mechanical framework based on HEOM formulated within an atomic orbital (AO) basis. The code enables numerically “exact” simulations of atomic systems coupled to 3D environments while preserving rotational symmetry. The inclusion of full spatial degrees of freedom introduces significant computational challenges, stemming from the proliferation of electronic states at elevated temperatures and the expansion of temperature-dependent HEOM terms at low temperatures. To address these demands, we developed software optimized for Graphics Processing Units (GPUs). Although primarily designed for atomic systems, the program is readily applicable to molecular electronic orbitals and intramolecular vibrational dynamics involving multiple interacting modes.

This paper is organized as follows. Section II introduces the 3D-RISB model for atomic electronic states and presents the AO-HEOM framework. The atomic electronic states employed in the simulations are briefly described. Section III outlines the structure of the source code. A numerical demonstration for He I and II is provided in Sec. IV. Finally, Sec. V concludes with a summary and outlook.

II. FORMULATION

A. The RISB model

An environment of a system described in atomic orbitals that have to satisfy rotational invariance can be modeled using a 3D-RISB model.^{51,54} We consider the total system expressed as

$$\hat{H}_{tot} = \hat{H}_S + \sum_{\alpha} \hat{H}_{I+B}^{\alpha}, \quad (1)$$

where the primary system represents a nonrelativistic atomic Hamiltonian. For a system of N electrons, this is expressed as

$$\hat{H}_S = \sum_{i=1}^N \left(-\frac{\hbar^2}{2m_e} \nabla_i^2 - \frac{Ze^2}{4\pi\epsilon_0 r_i} \right) + \sum_{i<j}^N \frac{e^2}{4\pi\epsilon_0 |\mathbf{r}_i - \mathbf{r}_j|}, \quad (2)$$

where \mathbf{r}_i denotes the position vector of the i th electron, Z is the atomic charge, e is the elementary charge, m_e is the electron mass, \hbar is the Planck constant, and ϵ_0 is the vacuum permittivity. The Laplacian operator ∇_i^2 acts on the spatial coordinates of electron i . The Hamiltonian comprises the electronic kinetic energy, the attractive Coulomb interaction between electrons and nuclei, and the repulsive Coulomb interaction among electrons.

The primary system is coupled to α -independent baths. The system–bath (S–B) interaction and bath Hamiltonian are then expressed as

$$\hat{H}_{I+B}^{\alpha} = \sum_j \left\{ \frac{(\hat{p}_j^{\alpha})^2}{2m_j^{\alpha}} + \frac{1}{2} m_j^{\alpha} (\omega_j^{\alpha})^2 \left(\hat{q}_j^{\alpha} - \frac{c_j^{\alpha} \hat{V}_{\alpha}}{m_j^{\alpha} (\omega_j^{\alpha})^2} \right)^2 \right\}, \quad (3)$$

where m_j^{α} , \hat{p}_j^{α} , \hat{q}_j^{α} , and ω_j^{α} represent the mass, momentum, coordinate, and frequency, respectively, of the j th bath oscillator mode in the α direction. The system part of the S–B interaction is described as V_{α} . In systems with rotational symmetry, the index α runs over x , y , and z , and the operators $(\hat{V}_x, \hat{V}_y, \hat{V}_z)$ are, in a simple case, identified with the position operators $(\hat{x}, \hat{y}, \hat{z})$ as in the 3D-RISB model for a quantum rotor.^{50,51,55}

We include the counterterms that are introduced to maintain the translational symmetry of the system Hamiltonian.¹⁹ The harmonic bath in the α direction is characterized by the spectral distribution function (SDF), defined as $J^{\alpha}(\omega) = \sum_k [\hbar(c_k^{\alpha})^2 / 2m_k^{\alpha} \omega_k^{\alpha}] \delta(\omega - \omega_k^{\alpha})$, and the inverse temperature, $\beta \equiv 1/k_B T$, where k_B is the Boltzmann constant.

B. Atomic electronic states for 3D-RISB model

The Hamiltonian introduced above underlies many electronic structure theories, such as Hartree–Fock (HF) and density functional theory. When applying the HEOM formalism, the atomic orbitals derived from these methods can be adopted as eigenstates for constructing the system Hamiltonian.

To obtain the input \hat{H}_S and \hat{V}_{α} matrices from quantum chemistry, we employ Psi4, an open-source quantum chemistry library written in Python.⁵⁶ As a prototypical example, we outline the procedure for computing atomic electronic structures using helium and

provide a concise summary of the quantum-chemical framework presented in [Appendices A](#) and [B](#), as follows:

- Specify the atomic basis set and the HF method to be employed.
- Perform the HF calculation to determine the orbitals.
- Postprocess the Hamiltonian using the HF orbitals to obtain post-HF orbitals.
- Evaluate \hat{H}_S and \hat{V}_α in the post-HF orbital basis and provide the matrix elements.

The methodology for constructing electronic orbitals in HEOM is presented in greater detail in molecular orbital (MO) investigations (MO-HEOM), in which the influence of intramolecular vibrations is taken into account.⁵⁷

C. AO-HEOM

The method we use to solve the dynamics of the reduced density operator is the HEOM, which provides a non-Markovian approach to numerically accurate solutions even in the strong S-B interaction case.^{12,13,17,21}

To adapt the standard HEOM formalism, we use the Drude SDF expressed as^{12,13}

$$J^\alpha(\omega) = \frac{\hbar\eta_\alpha}{\pi} \frac{\gamma_\alpha^2\omega}{\gamma_\alpha^2 + \omega^2}, \quad (4)$$

where $\alpha = x, y,$ and z . It should be noted that $J^\alpha(\omega)$ does not have to be identical for different α directions. In particular, they will differ when the surrounding environment is anisotropic. Such a situation can also be achieved by applying a Stark electric field in a specific direction.⁵¹ If necessary, we can also set anisotropic environments, for example, in the xy direction by correlating the bath modes in the $\alpha = x$ and y directions.⁵⁸

The hierarchical structure was introduced to describe the entanglement that arises from multiple interactions with the heat bath.^{12,13} In this paper, we adopt the $[K_\alpha - 1/K_\alpha]$ Padé approximation, where K_α is an integer in the α direction, to express the fluctuation and dissipation operators.⁵⁹ The HEOM in terms of Padé approximated frequency v_k^α , where $k = \{0, 1, \dots, K_\alpha\}$ with $v_0^\alpha = \gamma_\alpha$, are then expressed as^{50,51}

$$\begin{aligned} \frac{d}{dt}\hat{\rho}_{\{\mathbf{n}_\alpha\}} = & -\left[\frac{i}{\hbar}\hat{H}_S^\times + \sum_{\alpha=x,y,z} \sum_{k=0}^{K_\alpha} (n_k^\alpha v_k^\alpha)\right]\hat{\rho}_{\{\mathbf{n}_\alpha\}} \\ & - \frac{i}{\hbar} \sum_{\alpha=x,y,z} \sum_{k=0}^{K_\alpha} n_k^\alpha \hat{\Theta}_k^\alpha \hat{\rho}_{\{\mathbf{n}_\alpha - \mathbf{e}_\alpha^k\}} \\ & - \frac{i}{\hbar} \sum_{\alpha=x,y,z} \sum_{k=0}^{K_\alpha} \hat{V}_\alpha^\times \hat{\rho}_{\{\mathbf{n}_\alpha + \mathbf{e}_\alpha^k\}}, \end{aligned} \quad (5)$$

where $\{\mathbf{n}_\alpha\} \equiv (\mathbf{n}_x, \mathbf{n}_y, \mathbf{n}_z)$ is a set of integers $\mathbf{n}_\alpha = (n_0^\alpha, n_1^\alpha, n_2^\alpha, \dots, n_{K_\alpha}^\alpha)$ to describe the hierarchy elements and $\{\mathbf{n}_\alpha \pm \mathbf{e}_\alpha^k\}$ with the index k , where \mathbf{e}_α^k is the k th unit vector in the α direction. We introduced the hyperoperators $\hat{A}^\times \hat{B} \equiv \hat{A}\hat{B} - \hat{B}\hat{A}$ and $\hat{A}^\circ \hat{B} \equiv \hat{A}\hat{B} + \hat{B}\hat{A}$ for any operators \hat{A} and \hat{B} , and $\hat{\Theta}_k^\alpha$ is defined as

$$\hat{\Theta}_0^\alpha = \frac{\eta_\alpha \gamma_\alpha}{\beta} \left(1 + \sum_{k=1}^{K_\alpha} \frac{2\eta_k \gamma_k^\alpha}{\gamma_\alpha^2 - v_k^{\alpha 2}} \right) \hat{V}_\alpha^\times - \frac{\eta_\alpha \gamma_\alpha}{2} (\hat{H}_S^\times \hat{V}_\alpha)^\circ \quad (6)$$

and

$$\hat{\Theta}_{k \neq 0}^\alpha = -\frac{\eta_\alpha \gamma_\alpha^2}{\beta} \frac{2\eta_k v_k^\alpha}{\gamma_\alpha^2 - v_k^{\alpha 2}} \hat{V}_\alpha^\times, \quad (7)$$

where β , η_α , and γ_α are the inverse temperature, anisotropic coupling strength, and bath parameter, respectively. In Eq. (5), $\hat{\rho}_{\{\mathbf{n}_\alpha\}}$ are auxiliary operators with a hierarchical structure. The zeroth member of the hierarchical elements, $\hat{\rho}_{\{\mathbf{n}_\alpha=0\}}$, represents the original reduced density operator. As $(\mathbf{n}_x, \mathbf{n}_y, \mathbf{n}_z)$ can take all combinations of non-negative integers, the HEOM must be closed by introducing various forms of “terminators.”^{13,19,60} Here, we employ the form described in Ref. 21,

$$\sum_{\alpha=x,y,z} \sum_{k=0}^{K_\alpha} (n_k^\alpha v_k^\alpha) \hat{\rho}_{\{\mathbf{n}_\alpha\}} = -\frac{i}{\hbar} \sum_{\alpha=x,y,z} \sum_{k=0}^{K_\alpha} n_k^\alpha \hat{\Theta}_k^\alpha \hat{\rho}_{\{\mathbf{n}_\alpha - \mathbf{e}_\alpha^k\}}, \quad (8)$$

for $\sum_{\alpha=x,y,z} \sum_{k=0}^{K_\alpha} (n_k^\alpha v_k^\alpha) \gg \Delta\omega_{\max}$, where $\Delta\omega_{\max}$ is the largest transition frequency.

D. Emission spectra

Our previous studies examined the absorption spectrum of hydrogen atoms as a representative case, owing to their relatively low excitation energies, which give rise to numerous spectral lines even at low temperatures.⁵⁴ In this paper, we focus on emission spectra, which are widely used in atomic spectroscopy and play a crucial role in identifying and characterizing the atomic constituents of stars, where thermal excitation effects become significant.

The dipole operators of the atomic system are expressed in polar coordinates as $\hat{\mu}_x = \mu_0 \sin(\theta) \cos(\phi)$, $\hat{\mu}_y = \mu_0 \sin(\theta) \sin(\phi)$, and $\hat{\mu}_z = \mu_0 \cos(\theta)$. The emission spectrum considered in this study is defined as follows:¹²

$$I_{\alpha'}^{\text{(em)}}(\omega) = \text{Re} \int_0^\infty dt e^{i\omega t} \text{Tr} \{ \hat{\mu}_\alpha^- \hat{G}(t) (\hat{\rho}^{\text{eq}} \hat{\mu}_{\alpha'}^+) \}, \quad (9)$$

where $\hat{G}(t)$ is the Green's function in the absence of a laser interaction, evaluated from Eq. (5), and $\hat{\rho}^{\text{eq}}$ is the equilibrium density operator. In the reduced equation of motion approach, the density matrix is replaced by a reduced one. In the HEOM case, $\hat{\rho}^{\text{eq}}$ is replaced by the hierarchy member $\hat{\rho}_{\{\mathbf{n}_\alpha\}}^{\text{eq}}(t)$. The Liouvillian in $\hat{G}(t)$ is replaced using Eqs. (5)–(8). The dipole operator is divided into absorption and emission components as $\hat{\mu}_\alpha = \hat{\mu}_\alpha^+ + \hat{\mu}_\alpha^-$, where

$$\hat{\mu}_\alpha^+ = \sum_{E_m > E_n} \mu_\alpha^{mn} |m\rangle \langle n| \quad (10)$$

and

$$\hat{\mu}_\alpha^- = \sum_{E_m < E_n} \mu_\alpha^{mn} |m\rangle \langle n| \quad (11)$$

with the atomic energy eigenstates of energies E_n and E_m expressed as $|n\rangle$ and $|m\rangle$, respectively. The transition dipole component is defined as $\mu_\alpha^{mn} = \langle m | \hat{\mu}_\alpha | n \rangle$. It should be noted that we disregard the μ_α^{mn} elements when $E_n = E_m$, since no electronic transition occurs in this case.

To compute the emission spectrum in Eq. (9), we solve the HEOM starting from the initial equilibrium state at $t = 0$, given by $\hat{\rho}^{\text{eq}} \hat{\mu}_\alpha^+$. The solution at time t is denoted by $\hat{\rho}'(t)$, and we then compute the expectation value: $\text{tr}\{\hat{\mu}_\alpha^- \hat{\rho}'(t)\}$. The emission spectrum is finally obtained by performing the Fourier transform of this quantity.

For reference, we also present the emission spectrum in the absence of S–B coupling. According to Fermi's golden rule, the emission intensity is given by

$$I_{\alpha\alpha}^{(\text{em})}(\omega) = \sum_{E_n > E_m} \mu_\alpha^{mn} \mu_\alpha^{nm} \frac{e^{-\beta E_n}}{Z} \delta(\hbar\omega - (E_n - E_m)), \quad (12)$$

where $Z = \sum_n e^{-\beta E_n}$ is the partition function. This expression describes spontaneous emission from thermally populated excited states and serves as a reference for evaluating bath-induced spectral modifications.

III. AO-HEOM: SOFTWARE AND REQUIREMENTS

AO-HEOM is a Python program with GPU acceleration for simulating excited-state electron dynamics in 3D baths, developed to compute absorption and emission spectra by incorporating the time evolution of the reduced density operator. To perform simulations, users must specify the system Hamiltonian \hat{H}_S and the system component of the system–bath interaction \hat{V}_α , as described in Sec. II B and Appendices A and B.

Execution requires an NVIDIA GPU and the CUDA Toolkit. Our benchmark system employed an Intel Core i9-13900KF CPU, an NVIDIA GeForce RTX 4090 GPU, and CUDA Toolkit version 11.8. We used Python 3.13.5 on Windows 11, with CuPy 13.4.1 for CUDA support, NumPy 2.2.5, and SciPy 1.15.3 for special functions and numerical integration. To obtain a matrix representation of the Hamiltonian and the system part of the S–B interaction, we employ the SciPy quad function, which is based on the FORTRAN QUADPACK library.

Time evolution of the HEOM was performed using the fourth-order Runge–Kutta method. Although the code structure is simple, it efficiently manages large queues via external libraries.

Details of the AO-HEOM algorithm are provided in the accompanying README.pdf file.

This code is applicable to any system formulated within the 3D-RISB framework, provided that the system Hamiltonian and S–B interaction operators are expressed in matrix form with respect to an arbitrary basis. Consequently, it can be employed for atomic systems, the 3D rotor, and molecular systems in the absence of nuclear vibrations. Although our demonstrations for hydrogen and helium employ isotropic baths owing to their spherical symmetry, the AO-HEOM code is capable of describing spatial anisotropy in relaxation.⁵¹ To achieve a more sophisticated representation, the number of baths may be increased as needed and, if required, SDFs can be specified to account for correlations among baths.⁵⁸

IV. NUMERICAL DEMONSTRATION: HE I AND II

We apply the present method to the computation of the emission spectra of He I and He II, thereby demonstrating its capability to treat atoms with distinct excited states and spectral characteristics. He II, a hydrogen-like ion formed by the ionization of neutral helium (He I), possesses energy levels that scale with the square of the nuclear charge. Consequently, its effective Rydberg constant is four times larger than that of hydrogen, whose absorption spectrum was examined in our previous study.⁵⁴ For multi-electron systems such as He I, exact analytical solutions are unavailable; however, various quantum chemistry software packages can be employed to perform numerical calculations. Transition frequencies obtained from the quantum chemistry calculations explained in Appendices A and B are presented in Table I.

After expressing \hat{H}_S and \hat{V}_α ($\alpha = x, y, z$) in matrix form, the AO-HEOM program is initiated. Although the AO-HEOM can accommodate arbitrary forms of \hat{V}_α , we here assume $\hat{V}_\alpha = \hat{\mu}_\alpha$, corresponding to the standard electromagnetic interaction.

Since He atoms possess spherical symmetry, we consider an isotropic bath scenario in which the coupling strengths are uniform across all spatial directions: $\eta_x = \eta_y = \eta_z = \eta$. The inverse noise correlation times are all fixed to $\gamma_x = \gamma_y = \gamma_z = 1$. The spectra presented in Fig. 1 were obtained using Eq. (9). The number of hierarchical layers for each heat bath was set to $N_\alpha = 2$ for $\eta = 0.01$ and $N_\alpha = 1$ for $\eta = 0.001$ using the Padé approximation of the [2/3] form for He I and the [4/5] form for He II, for both $\beta = 3$ and 5.

TABLE I. The transition frequencies of He I between the singlet states Γ' and Γ were calculated using the quantum chemistry results presented in Table II (in atomic units). Values without a star mark indicate forbidden transitions. The calculated and experimental results⁵¹ are in close agreement: 0.7837 vs 0.7797 for $1s2p \rightarrow 1s1s$, 0.0267 vs 0.0221 for $1s2p \rightarrow 1s2s$, and 0.0737 vs 0.0626 for $1s3s \rightarrow 1s2p$. Due to basis-set limitations, the deviation of the calculated transition frequencies from the observed values becomes larger for higher excitations.

$\Gamma \backslash \Gamma'$	1s2s	1s2p	1s3s	1s3d	1s3p
1s1s	0.7570	0.7837*	0.8573	0.9964	1.0757*
1s2s		0.0267*	0.1003	0.2395	0.3187*
1s2p			0.0737*	0.2128*	0.2920
1s3s				0.1391	0.2186*
1s3d					0.0792*

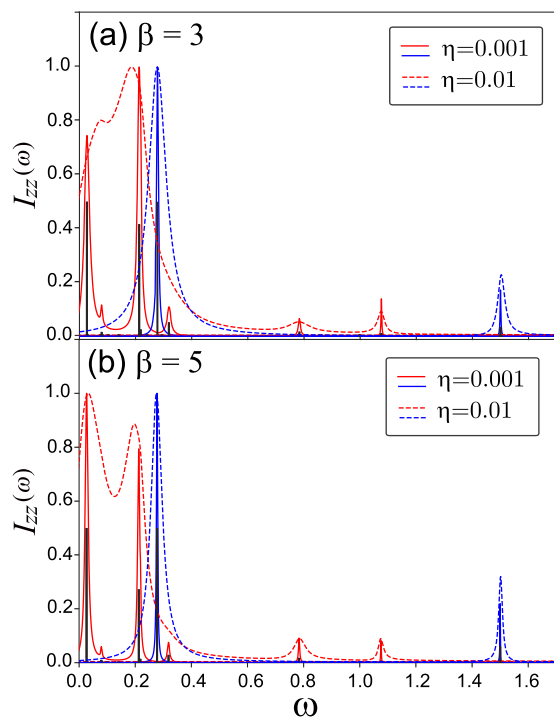


FIG. 1. Emission spectra $I_{zz}(\omega)$ in the z direction for He I (red curves) and He II (blue curves) at different S–B coupling strengths: (i) weak (solid curve, $\eta = 0.001$) and (ii) moderate (dashed curve, $\eta = 0.01$). Panel (a) corresponds to high temperature ($\beta = 3.0$), while panel (b) corresponds to low temperature ($\beta = 5.0$). Each spectrum is normalized to its maximum value, while the results obtained from Fermi's golden rule for He I and He II are scaled to 0.5 so as not to disrupt the AO-HEOM results. For comparison with the AO-HEOM results, spectral peaks calculated from the golden rule [Eq. (12)] are shown for He I and He II as black vertical lines.

Using a PC with an NVIDIA GeForce RTX 4090 GPU, each simulation comprising 10^6 time steps consumed about 1.2 GB of GPU memory and took roughly 300 s to complete.

Figure 1 presents the emission spectra of He I (red curves) and He II (blue curves) at (a) high ($\beta = 3$) and (b) low temperatures ($\beta = 5$) for weak (solid) and moderately weak (dashes) S–B coupling strengths, respectively. For He systems, these inverse temperatures correspond to (a) 100 000 K and (b) 60 000 K.

Note that both He I and He II have higher excitation energies than hydrogen. At these temperatures, energy states above the 3^3D ($1s3d$) level of He I and the excited energy states of He II with $n \geq 4$ are scarcely populated. Therefore, their contributions to the emission spectrum can be neglected.

The major peaks of He I (red curves) correspond to the transitions $1s2p \rightarrow 1s2s$ (0.0267) and $1s3d \rightarrow 1s2p$ (0.2128), while the minor peaks arise from $1s3s \rightarrow 1s2p$ (0.0737), $1s3p \rightarrow 1s2s$ (0.3187), $1s2p \rightarrow 1s1s$ (0.7837), and $1s3p \rightarrow 1s1s$ (1.0757). The numbers in parentheses denote the transition frequencies listed in Table I. As evident from the table, the features near 0.21 and 0.07 consist of two closely spaced peaks.

Unlike the hydrogen atom, electron–electron repulsion lifts the degeneracy of states with the same principal quantum number, while

only transitions between states of different parity occur. Nevertheless, the overall features of the emission spectrum calculated by Fermi's golden rule remain largely unchanged: transitions to the s state exhibit the highest peaks within each series (e.g., transitions to $1s3s$ and $1s2s$ are stronger than those to $1s3d$ and $1s2p$), and series with lower transition frequencies generally show higher peaks than those with higher frequencies (e.g., $1s3p \rightarrow 1s2s$ is stronger than $1s3p \rightarrow 1s1s$).

For convenience, we adopt the same series nomenclature as used for the hydrogen atom to describe single-electron transitions in He I. Accordingly, the peaks $1s2p \rightarrow 1s1s$ (0.7837) and $1s3p \rightarrow 1s1s$ (1.0757) correspond to the Lyman series. The Paschen series appears at $1s3p \rightarrow 1s3s$ (0.2186) and $1s3p \rightarrow 1s3d$ (0.0792) in the last two rows. The remaining peaks, including the highest one, $1s2p \rightarrow 1s2s$ (0.0267), belong to the Balmer series.

The eigenstates of He II are the same as those of hydrogen, as shown in Ref. 54, except with $Z = 2$; hence, they will not be repeated. The spectral peaks (blue) observed in He II correspond to the Lyman and Balmer series of the hydrogen atom. Since He II has a Rydberg constant four times larger than that of the hydrogen atom, no other peaks have been observed.

As expected, the emission peaks broaden with increasing S–B coupling strength, especially in the low-frequency regime. As the temperature increases (i.e., as β decreases), spectral peaks exhibit further broadening due to enhanced thermal fluctuations. Additionally, slight blue shifts in peak positions are observed in the high-frequency region, reflecting an increased population of excited states at elevated temperatures.

In absorption spectra, atoms are promoted to higher energy levels by laser irradiation from the thermal equilibrium state,⁵⁴ whereas in emission spectra, transitions originate only from thermally populated lower levels. Consequently, the overall absolute intensity (i.e., the normalization coefficient) is affected in the opposite manner by increasing temperature. Apart from this distinction, the influence of the thermal bath on the spectral profile remains essentially similar.

The present findings are expected to facilitate detailed analyses of atomic thermal environments based on stellar emission spectra.

V. CONCLUSION

To date, open quantum dynamics theory has lacked a rigorous and general framework for describing quantum thermal interactions in spatially extended systems, including atomic electronic states. The source code provided herein was developed to bridge this gap, empowering researchers across disciplines—including atomic spectroscopy and quantum chemistry—to investigate quantum thermodynamic effects governed by fluctuations and dissipation, even in the absence of specialized expertise in open quantum dynamics theory.

Disregarding computational cost, once the density operator representing the excited state is obtained, along with the quantum Liouville operator governing its time evolution and the S–B interaction operators, a fully dynamical description becomes feasible, even under time-dependent external fields. This formalism naturally accommodates the computation of nonlinear optical responses, including multidimensional spectra,^{12,13} and permits the introduction of external fields as vector potentials,^{52,53} thereby expanding the range of physical phenomena that can be addressed.

The methodology is readily extensible to molecular systems described by molecular orbitals (MO-HEOM).⁵⁷ Whether one adopts atomic or molecular orbital representations, the central challenge remains the accurate description of electron excited-state dynamics. While the application of AO-HEOM increases computational cost, it provides substantial physical benefits: the thermal bath efficiently relaxes highly excited states and steers the wave packet toward thermal equilibrium, thereby shaping and stabilizing its structure with a reduced basis set. These effects go beyond mere temperature correction. The density matrix formalism of HEOM is also anticipated to integrate seamlessly with functional approaches such as time-dependent density functional theory (TDDFT), thereby facilitating the development of hybrid methods.

We anticipate that this framework will stimulate further developments and applications across a broad spectrum of fields, advancing the quantum mechanical treatment of thermodynamic phenomena in complex systems.

SUPPLEMENTARY MATERIAL

The [supplementary material](#) provides the AO-HEOM software along with demonstration codes illustrating the calculation of the emission spectra of He I and He II atoms. Comprehensive instructions can be found in the `ReadMe.tex` file.

ACKNOWLEDGMENTS

We are very grateful to Professor So Hirata for his indispensable help with the calculation of atomic electronic states. Y.Z. thanks Shoki Koyanagi for providing useful information in the development of the HEOM source code. Y.T. was supported by JST (Grant No. CREST 1002405000170). Y.Z. is supported by JST SPRING, the establishment of university fellowships toward the creation of science technology innovation (Grant No. JPMJSP2110).

AUTHOR DECLARATIONS

Conflict of Interest

The authors have no conflicts to disclose.

Author Contributions

Yankai Zhang: Data curation (lead); Formal analysis (equal); Software (lead); Writing – original draft (equal). **Yoshitaka Tanimura:** Conceptualization (lead); Formal analysis (equal); Funding acquisition (lead); Supervision (lead); Writing – original draft (equal); Writing – review & editing (lead).

DATA AVAILABILITY

The data that support the findings of this study are available from the corresponding author upon reasonable request.

APPENDIX A: ELECTRONIC EIGENSTATES OF ATOMS

1. One-electron wavefunctions

Within the single-determinant approximation, the total electronic wavefunction is represented by a Slater determinant

constructed from one-electron orbitals. These orbitals are obtained as solutions of the Hartree–Fock (HF) equations, derived from the variational principle.

In the limit of a complete basis, HF yields the optimal single-determinant description of the exact wavefunction. Because the Hilbert space is infinite-dimensional, practical implementations rely on finite Gaussian basis sets to approximate atomic orbitals (AOs), originally modeled by Slater-type orbitals (STOs).

2. Multi-electron wavefunctions

For an N -electron system, the Fock operator possesses infinitely many orthonormal eigenfunctions. In practice, a finite basis of dimension $2K > N$ provides only $2K$ orbitals. The corresponding orbital energies systematically overestimate the exact values, and the resulting HF wavefunction is not an eigenfunction of the true Hamiltonian. Nevertheless, this construction provides the foundation for correlation treatments.

The Hamiltonian matrix elements between determinants can be expressed in second quantization as

$$\langle a\bar{b}|\hat{O}|c\bar{d}\rangle = \delta_{ac}\langle\bar{b}|\hat{O}_1|\bar{d}\rangle + \delta_{i\bar{a}}\langle a|\hat{O}_1|c\rangle + \langle a\bar{b}|\hat{O}_2|c\bar{d}\rangle, \quad (\text{A1})$$

where \hat{O}_1 and \hat{O}_2 denote one- and two-electron operators, respectively. In the linear combination of atomic orbitals (LCAO) representation, an orbital is expressed as $|a\rangle = \sum_i C_{ia}|\chi_i\rangle$, where $|\chi_i\rangle$ denotes atomic basis functions and C_{ia} are the LCAO coefficients obtained from the HF procedure. The one-electron and two-electron matrix elements are

$$\langle a|\hat{O}_1|c\rangle = \sum_{ij} C_{ia}C_{jc}\langle i|\hat{O}_1|j\rangle, \quad (\text{A2})$$

$$\langle a\bar{b}|\hat{O}_2|c\bar{d}\rangle = \sum_{ijkl} C_{ia}C_{jb}C_{kc}C_{ld}\langle ij|\hat{O}_2|kl\rangle. \quad (\text{A3})$$

The LCAO approximation expresses molecular or atomic orbitals as linear combinations of localized atomic orbitals, thereby bridging atomic and molecular descriptions.

Correlation effects are often incorporated by Configuration Interaction (CI), which constructs approximate many-electron wavefunctions from a truncated set of Slater determinants. Full Configuration Interaction (FCI), by contrast, includes all possible determinants within the chosen orbital basis, yielding the exact solution of the nonrelativistic Schrödinger equation in that finite basis. Thus, CI provides a balance between efficiency and accuracy, while FCI serves as the benchmark for numerical exactness. For two-electron systems such as helium, FCI can be carried out straightforwardly, and the results coincide with the true eigenvalues within the chosen basis. For larger atoms and molecules, truncated CI is often adopted for computational feasibility.

Beyond CI, the Equation-of-Motion Coupled-Cluster Singles and Doubles (EOM-CCSD) method,^{62–65} coupled-cluster linear response (CC-LR),^{66–70} and symmetry-adapted-cluster configuration interaction (SAC-CI)^{71,72} are excited-state extensions of the coupled-cluster (CC) method⁷³ by applying excitation operators R_n to the correlated ground state $|\Phi_0\rangle$. Unlike CI, which diagonalizes the Hamiltonian in a truncated determinant space, EOM-CCSD employs the exponential ansatz e^T (with T containing single and double excitations) to incorporate dynamic correlation efficiently.

This yields accurate excitation energies and transition properties while maintaining size consistency and systematic improvement. In practice, EOM-CCSD is widely regarded as a reliable balance between accuracy and computational cost for small- to medium-sized systems. In the dual representation,

$$\langle R_n^{\text{EOM-CCSD}} \rangle = e^T R_n |\Phi_0\rangle \quad (\text{A4})$$

and

$$\langle L_n^{\text{EOM-CCSD}} \rangle = \langle \Phi_0 | L_n e^{-T}. \quad (\text{A5})$$

The Hamiltonian can be expanded to a diagonal form, although coordinate operators $\hat{X}, \hat{Y}, \hat{Z}$ remain non-Hermitian. For two-electron systems, EOM-CCSD is equivalent to FCI in energy calculations when excited states are fully computed using the Davidson method, and truncated expansions are acceptable as long as convergence is achieved.

3. Extension to systems with three or more electrons

For atoms and molecules containing three or more electrons, additional challenges arise. First, the Pauli principle requires careful construction of spin-adapted determinants to ensure correct overall symmetries. Second, electron correlation effects, which are absent in HF, become increasingly important.

In such cases, truncated CI, FCI, or EOM-CCSD can be employed, with the choice depending on the balance between accuracy and computational feasibility. While HF remains the essential starting point, reliable electronic-structure descriptions of systems with $N \geq 3$ electrons invariably demand correlation treatments beyond the mean-field level.

Comparisons of full and truncated CI with the EOM-CC method have been reported in numerous earlier studies,^{73,74} in which the frozen-core approximation is commonly employed.

APPENDIX B: HE I EIGENSTATES FOR AO-HEOM

Now we illustrate how to incorporate AO information into AO-HEOM calculations, using He I as an example to enable spectral analysis of atomic systems. We adopt atomic units (a.u.), defined by $1/4\pi\epsilon_0 = 1$, $e = 1$, and $m_e = 1$.

For two-electron systems, EOM-CCSD yields energies equivalent to FCI when excited states are fully computed using the Davidson method. Truncated expansions are acceptable as long as convergence is achieved. We employ the d-aug-cc-pvtz basis for near-exact calculations. The lowest twelve energies and their multiplicities are listed in Table II.

Because the two electrons have different spins, the antisymmetric and symmetric spin states $\alpha(1)\beta(2) \mp \alpha(2)\beta(1)$ can be generated, corresponding, respectively, to the singlet and one of the triplet states. These arise from the combination of the spin state with either a symmetric or antisymmetric spatial state.

For two-electron spatial states composed of the same one-electron spatial function [e.g., $1s(1)1s(2) \pm 1s(2)1s(1)$], the antisymmetric state vanishes, leaving only the singlet state. In contrast, for states built from different one-electron spatial functions [e.g., $1s(1)2p(2) \pm 1s(2)2p(1)$], the singlet and triplet states have close but distinct energies -2.1286 and -2.1169 , in accordance with Hund's rule.

TABLE II. Energies and multiplicities calculated by FCI with the d-aug-cc-pVTZ basis set. Numbers in parentheses denote multiplicities. Singlet (s) and triplet (t) are determined from Hund's rule.

1s1s(s)	-2.900 608 13(1)
1s2s(t)	-2.173 618 71(1)
1s2s(s)	-2.143 609 4(1)
1s2p(t)	-2.128 566 84(3)
1s2p(s)	-2.116 937 66(3)
1s3s(t)	-2.061 439 55(1)
1s3s(s)	-2.043 261 07(1)
1s3d(t)	-1.904 818 68(5)
1s3d(s)	-1.904 144 8(5)
1s3p(t)	-1.872 369 46(3)
1s3p(s)	-1.824 951 51(3)
1s4s(t)	-1.634 905 95(1)
1s4s(s)	-1.463 531 79(1)
1s4d(t)	-0.827 103 44(5)
1s4d(s)	-0.821 157 37(5)
2s2s(s)	-0.773 837 94(1)

With smaller basis sets (e.g., cc-pVDZ), the discrepancies become more pronounced. For example, the energies -0.3847 and -0.0140 are obtained, which nevertheless help distinguish states with identical spatial functions such as $|1s1s(s)\rangle$.

The transition frequencies calculated using Table II are shown in Table I. Earlier HEOM studies on hydrogen revealed that S-B coupling compresses high-energy transitions in Coulomb systems. Therefore, spectral calculations at finite temperature are directed toward the low-energy region.

HF, CCSD, and EOM-CCSD calculations are performed sequentially. Within Psi4, invoking EOM-CCSD automatically executes all preceding steps. Although EOM-CCSD is widely recognized as a reliable approach to excited-state calculations, its application requires particular care, since the non-Hermitian structure of the formalism can complicate interpretation, especially with respect to spectral properties and the orthogonality of the resulting states.

To generate AO-HEOM input files, we employed Psi4,⁵⁶ although comparable tasks can be accomplished with other quantum chemistry packages. The input specifies nuclear coordinates, charge, multiplicity, basis set, and output settings, with `return_wfn` set to `True` in order to obtain HF properties for subsequent post-processing in CI codes. For EOM-CCSD calculations, the method is designated as `eom-ccsd`, the reference chosen as RHF for singlet states, and the parameter `roots_per_irrep` adjusted to facilitate convergence.

The construction of the Hamiltonian and coordinate operators in the two-electron wavefunction space (essentially the CI framework) requires both one- and two-electron integrals. As indicated in Eqs. (A1)–(A3), the function `psi4.core.MintsHelper.ao_eri` extracts two-electron integrals in the AO basis, while `psi4.core.wfn.Ca` provides AO coefficients for each HF orbital. One-electron integrals are obtained from `psi4.core.wfn.H` and `psi4.core.MintsHelper.ao_dipole`, yielding the core Hamiltonian matrix and the dipole matrix in the chosen basis-set representation. Efficient evaluation of Einstein summations is achieved using `numpy.einsum`.

Once the Hamiltonian has been assembled, we apply `numpy.linalg.eigh` to compute its eigenvalues and eigenvectors. The use of `numpy.linalg.eig` may introduce instabilities, likely because numerical errors in quantum chemistry render the Hamiltonian matrix not perfectly Hermitian. To emphasize the low-energy sector, both the Hamiltonian and the coordinate operators are diagonalized by aligning their eigenvectors into a unitary transformation. The resulting states are then ordered from lowest to highest energy.

Finally, we extract the submatrices corresponding to the singlet and other low-energy states and store them as `.npy` files. These files serve as the input for AO-HEOM. In emission spectrum calculations, special care must be taken in the treatment of degeneracies. Numerical data with minute discrepancies should be manually adjusted to exact equality to ensure physically consistent results.

REFERENCES

- 1 R. K. Wangsness and F. Bloch, "The dynamical theory of nuclear induction," *Phys. Rev.* **89**, 728–739 (1953).
- 2 A. J. Leggett, S. Chakravarty, A. T. Dorsey, M. P. A. Fisher, A. Garg, and W. Zwerger, "Dynamics of the dissipative two-state system," *Rev. Mod. Phys.* **59**, 1–85 (1987).
- 3 M. O. Scully and W. E. Lamb, "Quantum theory of an optical maser. I. General theory," *Phys. Rev.* **159**, 208–226 (1967).
- 4 B. R. Mollow and M. M. Miller, "The damped driven two-level atom," *Ann. Phys.* **52**, 464–478 (1969).
- 5 A. O. Caldeira and A. J. Leggett, "Path integral approach to quantum Brownian motion," *Physica A* **121**, 587–616 (1983).
- 6 H. Grabert, P. Schramm, and G.-L. Ingold, "Quantum Brownian motion: The functional integral approach," *Phys. Rep.* **168**, 115–207 (1988).
- 7 W. Nagourney, J. Sandberg, and H. Dehmelt, "Shelved optical electron amplifier: Observation of quantum jumps," *Phys. Rev. Lett.* **56**, 2797–2799 (1986).
- 8 T. Sauter, W. Neuhauser, R. Blatt, and P. E. Toschek, "Observation of quantum jumps," *Phys. Rev. Lett.* **57**, 1696–1698 (1986).
- 9 J. C. Bergquist, R. G. Hulet, W. M. Itano, and D. J. Wineland, "Observation of quantum jumps in a single atom," *Phys. Rev. Lett.* **57**, 1699–1702 (1986).
- 10 W. E. Moerner and L. Kador, "Optical detection and spectroscopy of single molecules in a solid," *Phys. Rev. Lett.* **62**, 2535–2538 (1989).
- 11 G. R. Fleming and G. D. Scholes, "The development and applications of multidimensional biomolecular spectroscopy illustrated by photosynthetic light harvesting," *Q. Rev. Biophys.* **57**, e11 (2024).
- 12 Y. Tanimura, "Stochastic Liouville, Langevin, Fokker–Planck, and master equation approaches to quantum dissipative systems," *J. Phys. Soc. Jpn.* **75**, 082001 (2006).
- 13 Y. Tanimura, "Numerically 'exact' approach to open quantum dynamics: The hierarchical equations of motion (HEOM)," *J. Chem. Phys.* **153**, 020901 (2020).
- 14 R. Silbey and R. A. Harris, "Variational calculation of the dynamics of a two level system interacting with a bath," *J. Chem. Phys.* **80**, 2615–2617 (1984).
- 15 S. Koyanagi and Y. Tanimura, "Thermodynamic quantum Fokker–Planck equations and their application to thermostatic Stirling engine," *J. Chem. Phys.* **161**, 112501 (2024); [arXiv:2408.01083](https://arxiv.org/abs/2408.01083).
- 16 S. Koyanagi and Y. Tanimura, "Hierarchical equations of motion for multiple baths (HEOM-MB) and their application to Carnot cycle," *J. Chem. Phys.* **161**, 162501 (2024); [arXiv:2408.02249](https://arxiv.org/abs/2408.02249).
- 17 Y. Tanimura and R. Kubo, "Time evolution of a quantum system in contact with a nearly Gaussian-Markoffian noise bath," *J. Phys. Soc. Jpn.* **58**, 101–114 (1989).
- 18 Y. Tanimura, "Nonperturbative expansion method for a quantum system coupled to a harmonic-oscillator bath," *Phys. Rev. A* **41**, 6676–6687 (1990).
- 19 Y. Tanimura and P. G. Wolynes, "Quantum and classical Fokker-Planck equations for a Gaussian-Markovian noise bath," *Phys. Rev. A* **43**, 4131–4142 (1991).
- 20 Y. Tanimura and P. G. Wolynes, "The interplay of tunneling, resonance, and dissipation in quantum barrier crossing: A numerical study," *J. Chem. Phys.* **96**, 8485–8496 (1992).
- 21 A. Ishizaki and Y. Tanimura, "Quantum dynamics of system strongly coupled to low-temperature colored noise bath: Reduced hierarchy equations approach," *J. Phys. Soc. Jpn.* **74**, 3131–3134 (2005).
- 22 N. Makri, "Numerical path integral techniques for long time dynamics of quantum dissipative systems," *J. Math. Phys.* **36**, 2430–2457 (1995).
- 23 N. Makri and D. E. Makarov, "Tensor propagator for iterative quantum time evolution of reduced density matrices. I. Theory," *J. Chem. Phys.* **102**, 4600–4610 (1995).
- 24 N. Makri and D. E. Makarov, "Tensor propagator for iterative quantum time evolution of reduced density matrices. II. Numerical methodology," *J. Chem. Phys.* **102**, 4611–4618 (1995).
- 25 Y. Fujihashi, G. R. Fleming, and A. Ishizaki, "Impact of environmentally induced fluctuations on quantum mechanically mixed electronic and vibrational pigment states in photosynthetic energy transfer and 2D electronic spectra," *J. Chem. Phys.* **142**, 212403 (2015).
- 26 K. Nakamura and Y. Tanimura, "Optical response of laser-driven charge-transfer complex described by Holstein–Hubbard model coupled to heat baths: Hierarchical equations of motion approach," *J. Chem. Phys.* **155**, 064106 (2021); [arXiv:2107.13194](https://arxiv.org/abs/2107.13194).
- 27 J. Jin, S. Welack, J. Luo, X.-Q. Li, P. Cui, R.-X. Xu, and Y. Yan, "Dynamics of quantum dissipation systems interacting with fermion and boson grand canonical bath ensembles: Hierarchical equations of motion approach," *J. Chem. Phys.* **126**, 134113 (2007).
- 28 R. Härtle, G. Cohen, D. R. Reichman, and A. J. Millis, "Decoherence and lead-induced interdot coupling in nonequilibrium electron transport through interacting quantum dots: A hierarchical quantum master equation approach," *Phys. Rev. B* **88**, 235426 (2013).
- 29 M. Thoss and F. Evers, "Perspective: Theory of quantum transport in molecular junctions," *J. Chem. Phys.* **148**, 030901 (2018).
- 30 T. Ikeda and Y. Tanimura, "Phase-space wavepacket dynamics of internal conversion via conical intersection: Multi-state quantum Fokker-Planck equation approach," *Chem. Phys.* **515**, 203–213 (2018).
- 31 R. Martinazzo, B. Vacchini, K. H. Hughes, and I. Burghardt, "Communication: Universal Markovian reduction of Brownian particle dynamics," *J. Chem. Phys.* **134**, 011101 (2011).
- 32 D. Tamascelli, A. Smirne, S. F. Huelga, and M. B. Plenio, "Nonperturbative treatment of non-Markovian dynamics of open quantum systems," *Phys. Rev. Lett.* **120**, 030402 (2018).
- 33 N. Lambert, S. Ahmed, M. Cirio, and F. Nori, "Modelling the ultra-strongly coupled spin-boson model with unphysical modes," *Nat. Commun.* **10**, 3721 (2019).
- 34 G. Pleasance, B. M. Garraway, and F. Petruccione, "Generalized theory of pseudomodes for exact descriptions of non-Markovian quantum processes," *Phys. Rev. Res.* **2**, 043058 (2020).
- 35 P. Menczel, K. Funo, M. Cirio, N. Lambert, and F. Nori, "Non-Hermitian pseudomodes for strongly coupled open quantum systems: Unravelings, correlations, and thermodynamics," *Phys. Rev. Res.* **6**, 033237 (2024).
- 36 Q. Shi and E. Geva, "A self-consistent treatment of electron transfer in the limit of strong friction via the mixed quantum classical Liouville method," *J. Chem. Phys.* **131**, 034511 (2009).
- 37 Q. Shi, Y. Xu, Y. Yan, and M. Xu, "Efficient propagation of the hierarchical equations of motion using the matrix product state method," *J. Chem. Phys.* **148**, 174102 (2018).
- 38 T. Ikeda and G. D. Scholes, "Generalization of the hierarchical equations of motion theory for efficient calculations with arbitrary correlation functions," *J. Chem. Phys.* **152**, 204101 (2020).
- 39 T. Ikeda and A. Nakayama, "Collective bath coordinate mapping of 'hierarchy' in hierarchical equations of motion," *J. Chem. Phys.* **156**, 104104 (2022).
- 40 Y.-T. Huang, P.-C. Kuo, N. Lambert, M. Cirio, S. Cross, S.-L. Yang, F. Nori, and Y.-N. Chen, "An efficient Julia framework for hierarchical equations of motion in open quantum systems," *Commun. Phys.* **6**, 313 (2023).
- 41 Y. Ke, "Tree tensor network state approach for solving hierarchical equations of motion," *J. Chem. Phys.* **158**, 211102 (2023).

- ⁴²R. Borrelli and S. Dolgov, "Expanding the range of hierarchical equations of motion by tensor-train implementation," *J. Phys. Chem. B* **125**, 5397–5407 (2021).
- ⁴³H. Takahashi and R. Borrelli, "Tensor-train format hierarchical equations of motion formalism: Charge transfer in organic semiconductors via dissipative Holstein models," *J. Chem. Theory Comput.* **20**, 7052–7064 (2024).
- ⁴⁴X. Chen and I. Franco, "Bexcitonics: Quasiparticle approach to open quantum dynamics," *J. Chem. Phys.* **160**, 204116 (2024).
- ⁴⁵X. Chen and I. Franco, "Tree tensor network hierarchical equations of motion based on time-dependent variational principle for efficient open quantum dynamics in structured thermal environments," *J. Chem. Phys.* **163**, 104109 (2025).
- ⁴⁶Z. Shi, H. Zhou, L. Huang, R. Xie, and L. Wang, "Hierarchical equations of motion solved with the multiconfigurational Ehrenfest ansatz," *J. Chem. Phys.* **163**, 224103 (2025).
- ⁴⁷Y. Suzuki and Y. Tanimura, "Quantum theory of a two-dimensional rotator in a dissipative environment: Application to far-infrared spectroscopy," *J. Phys. Soc. Jpn.* **70**, 1167–1170 (2001).
- ⁴⁸Y. Suzuki and Y. Tanimura, "Two-time correlation function of a two-dimensional quantal rotator in a colored noise," *J. Phys. Soc. Jpn.* **71**, 2414–2426 (2002).
- ⁴⁹Y. Gefen, E. Ben-Jacob, and A. O. Caldeira, "Zener transitions in dissipative driven systems," *Phys. Rev. B* **36**, 2770–2782 (1987).
- ⁵⁰Y. Iwamoto and Y. Tanimura, "Linear absorption spectrum of a quantum two-dimensional rotator calculated using a rotationally invariant system-bath Hamiltonian," *J. Chem. Phys.* **149**, 084110 (2018).
- ⁵¹Y. Iwamoto and Y. Tanimura, "Open quantum dynamics of a three-dimensional rotor calculated using a rotationally invariant system-bath Hamiltonian: Linear and two-dimensional rotational spectra," *J. Chem. Phys.* **151**, 044105 (2019).
- ⁵²H. Yang, S. Koyanagi, and Y. Tanimura, "Quantum hierarchical Fokker–Planck equations with U(1) gauge fields: Application to the Aharonov–Bohm ring," *J. Chem. Phys.* **163**, 144107 (2025).
- ⁵³S. Koyanagi, H. Yang, and Y. Tanimura, "Quantum hierarchical Fokker–Planck equations with U(1) gauge fields [U(1)-QHFP]: A computational framework for Aharonov–Bohm effects," *J. Chem. Phys.* **163**, 222502 (2025).
- ⁵⁴Y. Zhang and Y. Tanimura, "Open quantum dynamics theory for Coulomb potentials: Hierarchical equations of motion for atomic orbitals (AO-HEOM)," *J. Chem. Phys.* **163**, 184108 (2025).
- ⁵⁵L. Chen, M. F. Gelin, and W. Domcke, "Orientational relaxation of a quantum linear rotor in a dissipative environment: Simulations with the hierarchical equations-of-motion method," *J. Chem. Phys.* **151**, 034101 (2019).
- ⁵⁶D. G. A. Smith, L. A. Burns, A. C. Simmonett, R. M. Parrish, M. C. Schieber, R. Galvelis, P. Kraus, H. Kruse, R. Di Remigio, A. Alenaizan, A. M. James, S. Lehtola, J. P. Misiewicz, M. Scheurer, R. A. Shaw, J. B. Schriber, Y. Xie, Z. L. Glick, D. A. Sirianni, J. S. O'Brien, J. M. Waldrop, A. Kumar, E. G. Hohenstein, B. P. Pritchard, B. R. Brooks, H. F. Schaefer III, A. Y. Sokolov, K. Patkowski, A. E. DePrince III, U. Bozkaya, R. A. King, F. A. Evangelista, J. M. Turney, T. D. Crawford, and C. D. Sherrill, "Psi4 1.4: Open-source software for high-throughput quantum chemistry," *J. Chem. Phys.* **152**, 184108 (2020).
- ⁵⁷Y. Zhang, Y. Tanimura, and S. Hirata, "Molecular description of thermal activation and diffusion: Hierarchical equations of motion for molecular orbitals (MO-HEOM)," *arXiv:2512.22962* [Physics.chem-Ph] (2025).
- ⁵⁸H. Takahashi and Y. Tanimura, "Open quantum dynamics theory of spin relaxation: Application to μ SR and low-field NMR spectroscopies," *J. Phys. Soc. Jpn.* **89**, 064710 (2020).
- ⁵⁹J. Hu, R.-X. Xu, and Y. Yan, "Communication: Padé spectrum decomposition of Fermi function and Bose function," *J. Chem. Phys.* **133**, 101106 (2010).
- ⁶⁰X. Ding, D. Zhang, L. Ye, X. Zheng, and Y. Yan, "On the practical truncation tier of fermionic hierarchical equations of motion," *J. Chem. Phys.* **157**, 224107 (2022).
- ⁶¹A. Kramida, Y. Ralchenko, J. Reader, and NIST ASD Team, NIST Atomic Spectra Database (ver. 5.12), National Institute of Standards and Technology, Gaithersburg, MD, 2024, <https://physics.nist.gov/asd>.
- ⁶²K. Emrich, "An extension of the coupled cluster formalism to excited states (I)," *Nucl. Phys. A* **351**, 379–396 (1981).
- ⁶³K. Emrich, "An extension of the coupled cluster formalism to excited states: (II). Approximations and tests," *Nucl. Phys. A* **351**, 397–438 (1981).
- ⁶⁴H. Sekino and R. J. Bartlett, "A linear response, coupled-cluster theory for excitation energy," *Int. J. Quantum Chem.* **26**(S18), 255–265 (1984).
- ⁶⁵J. Geertsen, M. Rittby, and R. J. Bartlett, "The equation-of-motion coupled-cluster method: Excitation energies of Be and CO," *Chem. Phys. Lett.* **164**(1), 57–62 (1989).
- ⁶⁶S. Ghosh, D. Mukherjee, and S. Bhattacharyya, "Application of linear response theory in a coupled cluster framework for the calculation of ionization potentials," *Mol. Phys.* **43**(1), 173–179 (1981).
- ⁶⁷M. Takahashi and J. Paldus, "Time-dependent coupled cluster approach: Excitation energy calculation using an orthogonally spin-adapted formalism," *J. Chem. Phys.* **85**, 1486–1501 (1986).
- ⁶⁸H. Koch and P. Jørgensen, "Coupled cluster response functions," *J. Chem. Phys.* **93**, 3333–3344 (1990).
- ⁶⁹H. Koch, H. J. A. Jensen, P. Jørgensen, and T. Helgaker, "Excitation energies from the coupled cluster singles and doubles linear response function (CCSDLR). Applications to Be, CH⁺, CO, and H₂O," *J. Chem. Phys.* **93**, 3345–3350 (1990).
- ⁷⁰R. J. Rico and M. Head-Gordon, "Single-reference theories of molecular excited states with single and double substitutions," *Chem. Phys. Lett.* **213**, 224–232 (1993).
- ⁷¹H. Nakatsuji and K. Hirao, "Cluster expansion of the wave function. Electron correlations in singlet and triplet excited states, ionized states, and electron attached states by SAC and SAC–CI theories," *Int. J. Quantum Chem.* **20**, 1301–1313 (1981).
- ⁷²H. Nakatsuji, K. Ohta, and K. Hirao, "Cluster expansion of the wave function. Electron correlations in the ground state, valence and Rydberg excited states, ionized states, and electron attached states of formaldehyde by SAC and SAC–CI theories," *J. Chem. Phys.* **75**, 2952–2958 (1981).
- ⁷³S. Hirata, "Higher-order equation-of-motion coupled-cluster methods," *J. Chem. Phys.* **121**, 51–59 (2004).
- ⁷⁴S. Hirata, "Third- and fourth-order perturbation corrections to excitation energies from configuration interaction singles," *J. Chem. Phys.* **122**, 094105 (2005).